remote sensing

MDPI

Article

Design of a Grating Lobes-Free Architecture for Distributed Sensor System with Arbitrary Element Spacing

Jiyan Huang [1,*], Chaoyang Liu [1,2], Wei Hu [1] and Kuo Liao [1]

[1] School of Information and Communication Engineering, University of Electronic Science and Technology of China, Chengdu 611731, China; 202022011126@std.uestc.edu.cn (C.L.); 202021011122@std.uestc.edu.cn (W.H.); liaokuo@uestc.edu.cn (K.L.)

[2] State Key Laboratory of Complex Electromagnetic Environment Effects on Electronics and Information System (CEMEE), Changsha 410000, China

* Correspondence: huangjiyan@uestc.edu.cn

Abstract: Two main difficulties for the accurate direction of arrival (DOA) estimation in a distributed sensor system are grating lobes and system synchronization. Different from the traditional phased array system based on single carrier frequency, this paper designs a novel architecture for distributed sensor system using dual carrier frequency measurements. Both two carrier frequencies are combined and transmitted simultaneously in the proposed architecture. Instead of single carrier frequency f_1 in the traditional method, the frequency separation $f_2 - f_1$ is used in the proposed algorithm to determine a maximum unambiguous DOA estimate. Since $f_2 - f_1$ is much less than f_1 and the choice of $f_2 - f_1$ is more flexible, the proposed method can provide an unambiguous DOA estimate in the whole field of view (FOV) for arbitrary element spacing and a looser requirement on system synchronization than the traditional method based on single carrier frequency. For a case with $f_1 = 3$ Ghz, $f_2 - f_1 = 150$ Mhz and 10 times element spacing, there is no grating lobe for the proposed method in the whole FOV $[-\pi/2, \pi/2]$, whereas the traditional method has many grating lobes and the FOV of the traditional method without grating lobes is only 5.73°. To obtain the same combining efficiency in this case, the requirement on the positioning error of the proposed method is 0.4 m and the location error of the traditional method must be smaller than 0.02 m. Hence, the proposed method can greatly reduce hardware requirements. The performances of the proposed architecture for the cases with perfect and imperfect system synchronizations are evaluated in terms of the average beampattern and combining efficiency, respectively. Some characteristics of the derived beampattern and combining efficiency are also presented in the paper.

Keywords: distributed sensor system; beampattern; grating lobes; beamforming; combining efficiency; dual frequencies

Citation: Huang, J.; Liu, C.; Hu, W.; Liao, K. Design of a Grating Lobes-Free Architecture for Distributed Sensor System with Arbitrary Element Spacing. *Remote Sens.* **2022**, *14*, 1356. https://doi.org/10.3390/rs14061356

Academic Editor: Andrzej Stateczny

Received: 20 January 2022
Accepted: 4 March 2022
Published: 10 March 2022

1. Introduction

Array signal processing such as beamforming and direction of arrival (DOA) estimation using distributed sensor system has been a hot research topic in recent years Zaidi et al. [1]. It finds important and practical applications in many areas such as radars and wireless communications Jayaprakasam et al. [2], Diaz et al. [3]. Though adjusting the initial phase of each node to form a beam in the desired direction, the signal at the receiver becomes stronger and interference in other directions is reduced. Ideal transmit and receive joint beamforming with N antennas results in an N^3-fold gain in signal-to-noise ratio (SNR) Mudumbai et al. [4]. Joint beamforming can yield increased detection range (an $N^{3/4}$-fold increase for free space propagation) than a single-antenna sensor. In addition to SNR gain, distributed sensor systems with a large array aperture such as wireless sensor networks (WSN) and ad hoc sensor networks usually have the higher angular solution. In fact, beamforming and DOA estimation are not new and have been widely studied for phased-array active sensing system (e.g., radar, sonar, etc.) during the last 50 years.

Many researches including DOA Huang et al. [5], Nerea et al. [6], Lai et al. [7] and beamforming Droszcz et al. [8], Bollian et al. [9] algorithms, performance analysis Huang and Wan [10], Huang et al. [11], and array designs Manteghi and Blanco [12], Scholnik [13] have been the subject of an abundance of literature in phased array system. In addition to the above array signal processing algorithms, antenna systems are also very important and crucial for phased array system. Several antenna systems Alibakhshikenari et al. [14], Limiti [15], Althuwayb [16,17] have been reported in the literature and they provide hardware design basis for phased array system. Compared with the phased array system, there are two main difficulties in the distributed sensor system. The first one is the large distributed range. The element spacing in distributed sensor system is usually much larger than the half wave length which will lead to a lot of grating lobes and result in confusions on DOA estimation. Another important constraint on distributed sensor system is system synchronization. To combine the signals constructively at the destination, all of sensors should synchronize their carrier frequencies, time, and position. Due to the independent local oscillator (LO) and clock source in each sensor, it is very hard for a distributed sensor system to achieve a sufficient precision for system synchronization in a practical system.

Many grating lobes suppression algorithms have been proposed for phased array system in the literature. Dolph–Chebychev design approaches have been traditionally adopted to minimize sidelobe levels with respect to mainbeam width restrictions Andreasen [18], Viberg and Engdahl [19]. Subsequently, optimization strategies, including series expansions Unz [20], Ishimaru [21], simplex-type search Leahy and Jeffs [22], branch-and-bound techniques Holm et al. [23], genetic algorithms Haupt [24], simulated annealing Murino et al. [25] approaches, and iterative optimization algorithms Redlich [26], Mitrou [27], have been addressed in the literature to design receive antenna positions and beampattern weights. Sub-arrays separation techniques were presented in Chen and Chen [28], Chen et al. [29], Zoltowski and Wong [30], Li and Nehorai [31] to solve ambiguity in DOA estimate. Similar methods for grating lobes mitigating have been extended from the receive beamforming to multiple-input multiple-output (MIMO) systems Tu et al. [32], Roberts et al. [33].

Most of current studies Andreasen [18], Viberg and Engdahl [19], Unz [20], Ishimaru [21], Leahy and Jeffs [22], Holm et al. [23], Haupt [24], Murino et al. [25], Redlich [26], Mitrou [27], Chen and Chen [28], Chen et al. [29], Zoltowski and Wong [30], Li and Nehorai [31], Tu et al. [32], Roberts et al. [33] on grating lobes suppression are based on sensor position diversity technique. Unlike uniform linear array (ULA) or uniform circular array (UCA), random arrays with unequal element spacing in sensor position diversity techniques are designed to suppress grating lobes. Sensor position diversity technique has been successfully applied in a sparse array with narrow area distribution to obtain an unambiguous DOA estimate. For a distributed sensor system, it usually has a large distributed range where element spacing is hundreds or thousands of times more than wavelength. In this case, sidelobe levels of sensor position diversity technique becomes vary high and it is almost impossible to correctly detect a target in such high sidelobe level. System synchronization precision is another important factor which prevents sensor position diversity technique from applying in distributed sensor system. Since sensor position diversity technique is based on single carrier frequency, its synchronization errors should be at least less than sub-wavelength level. For example, the positioning error of a sensor with carrier frequency 3 Ghz should be less than 0.02 m for an acceptable combining efficiency. It is very hard for a distributed sensor system to reach such high location precision in the case with wide area distribution and dynamic environment.

In this paper, we design a novel grating lobes-free architecture for distributed sensor system with arbitrary element spacing. The performances of the proposed architecture for the cases with perfect and imperfect system synchronizations are also analyzed by theoretical derivation and simulation verification. Main contributions of this paper are listed as follows:

(1) This paper designs a novel grating lobes-free architecture for distributed sensor system with arbitrary element spacing. One of main difficulties of previous studies Jayaprakasam et al. [2], Diaz et al. [3], Mudumbai et al. [4], Li and Nehorai [31], Huang et al. [34], Ahmed and Vorobyov [35], Ochiai et al. [36], Anderson [37] based on single frequency measurements for distributed sensor system is grating lobe. To suppress grating lobes and obtain an unambiguous DOA estimate, element spacing in a traditional phased-array system Jayaprakasam et al. [2], Diaz et al. [3], Mudumbai et al. [4], Li and Nehorai [31], Huang et al. [34], Ahmed and Vorobyov [35], Ochiai et al. [36], Anderson [37] is set to be a half wave length. However, the element spacing in distributed sensor system is usually much larger than the half wave length which will lead to a lot of grating lobes and result in confusions on DOA estimation. Instead of the single carrier frequency f_1 in the traditional method, the frequency separation $f_2 - f_1$ is used in the proposed algorithm to determine a maximum unambiguous DOA estimate. Since $f_2 - f_1$ is much less than f_1 and the choice of $f_2 - f_1$ is more flexible, the proposed method can provide an unambiguous DOA estimate in the whole FOV for arbitrary element spacing. For a case with $f_1 = 3$ Hhz, $f_2 - f_1 = 150$ Mhz and 10 times element spacing, there is no grating lobe for the proposed method in the whole FOV $[-\pi/2, \pi/2]$, whereas the traditional method has many grating lobes and the FOV of the traditional method without grating lobes is only 5.73°. Obviously, it is impossible for the traditional method to be used in a practical system with such small FOV.

(2) Compared with the single frequency system, the proposed architecture provides a looser requirement on system synchronization with the same combining efficiency. In other words, the proposed architecture has the higher combining efficiency than the single frequency system with the same errors of system synchronization. This conclusion is proved in Proposition 3 and 4. For a case with the same combining efficiency, the requirement on the positioning error of the proposed method is 0.4 m, whereas the location error of the traditional method must be smaller than 0.02 m. Hence, the proposed method can greatly reduce hardware requirements.

(3) The average properties including 3 dB beamwidth, peak and zero points of the sidelobe, 3 dB sidelobe region, and average directivity are derived to evaluate the performance of the proposed architecture in the case of perfect system synchronization. Although those beampattern characteristics have been addressed for the single frequency architecture Huang et al. [34], Ahmed and Vorobyov [35], Ochiai et al. [36], the performance analysis on dual frequency architecture has not been studied in the literature to the best of our knowledge. Moreover, beampattern comparisons between the single carrier frequency architecture and the proposed design are also presented in the paper.

(4) The effects of the phase ambiguities caused by the imperfect system synchronization are evaluated in terms of the average combining efficiency. Both the average combining efficiencies of the traditional array radar based on single carrier frequency and the proposed architecture are derived for the case with imperfect phase. The average combining efficiency is a powerful tool to design a requirement on system synchronization. Considering a system with system parameters $f_2 - f_1 = 100$ Mhz, $f_0 = 10$ Mhz and $\sigma_\varphi < 26^\circ$, the requirements of system synchronization ($\sigma_x \leq 0.3$ m and $\sigma_f \leq 330$ khz) can be obtained using the proposed model of average combining efficiency.

This paper is organized as follows. Signal model and basic notations are presented in Section 2. In Section 3, the paper designs a novel grating lobes-free architecture for distributed sensor system with arbitrary element spacing. Section 4 derives the average properties of the proposed beampattern. Beampattern comparisons between the single carrier frequency architecture and the proposed design are also presented in this section. Section 5 analyzes the effects of the synchronization errors in terms of the average combining efficiency. Some characteristics of the derived combining efficiency are provided in the end of this section. Conclusions of this paper are given in Section 6.

2. System Model and Beampattern

The geometrical configuration of the distributed sensor system and destination (or target) is illustrated in Figure 1. In the figure, black dot is the sensor with a single antenna while black hexagon represents a far-field target. Range differences among the target and sensors will lead to phase differences between the adjacent sensors. For a far-field target, range differences can be modelled as a function containing the angle of the target. Hence, array signal processing algorithms use the phases differences collected from sensors for DOA estimation. Compared with the traditional methods based on phases differences from single carrier frequency, the proposed method utilizes the phases differences from dual frequencies to obtain an unambiguous DOA estimate in the whole FOV for arbitrary element spacing.

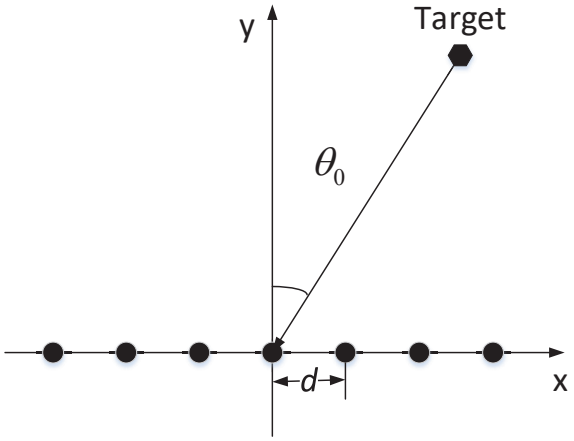

Figure 1. Target in the far-field of uniform linear array.

Assuming that θ_0 is the azimuth angle of a far-field target to be estimated and the known coordinate of the ith sensor in a N-sensors system is (x_i, y_i). For simplicity, we consider an ULA where the sensors are uniformly distributed in the interval $[-L/2, L/2]$. $L = (N-1)d$ is the array aperture, $d = m\lambda$ is the element spacing between sensors, and λ is the carrier wavelength of the signal. Without loss of generality, the array center is assumed to be at the origin O of this axis. Hence, the vertical axises of the sensors are 0 and the corresponding horizontal axises are $\mathbf{x} = [x_1, \cdots x_N]$ where $x_i = -L/2 + (i-1)d$. To suppress grating lobes and obtain an unambiguous DOA estimate, d is set to be $\lambda/2$ in a traditional phased-array radar. Compared with phased-array radar, the element spacing d of distributed sensor system is usually much larger than $\lambda/2$ which will lead to a large number of grating lobes.

The purpose of the paper is to design a distributed sensor system for removing the grating lobes in the case of $d \gg \lambda/2$. Beampattern is widely used for performance analysis of array radar. This describes the array gains at the different directions $\theta \in [-\pi/2, \pi/2]$. Generally, we can set $\theta_0 = 0$ where the target locates in the normal direction of the array. Synchronizing the carriers of the kth sensor node with initial phase $\psi_k = -2\pi x_k \sin(\theta_0)/\lambda$ for directional signal transmission or reception, the array factor of the traditional phased-array radar based on single carrier frequency is written as:

$$\begin{aligned} F(\theta) &= \frac{1}{N}\sum_{k=1}^{N} e^{j\psi_k} e^{j2\pi x_k \sin(\theta)/\lambda}|_{\theta_0=0} \\ &= \frac{1}{N}\sum_{k=1}^{N} e^{j2\pi x_k \sin(\theta)/\lambda} \\ &= \frac{1}{N}\sum_{k=1}^{N} e^{j2\pi(-L/2+(k-1)d)\sin(\theta)/\lambda} \end{aligned} \tag{1}$$

In (1), $\psi_k = -2\pi x_k \sin(\theta_0)/\lambda$ is the weight of beamforming algorithm and $2\pi x_k \sin(\theta)/\lambda$ is a actual phase for angle θ. Let $\theta = \theta_0$, $F(\theta)$ will have the maximum which is called mainlobe.

Substituting $d = m\lambda$ and $L = (N-1)d$ into (1), gives:

$$F(\theta) = \frac{1}{N}\sum_{k=1}^{N} e^{j2\pi(-(N-1)/2+(k-1))m\sin(\theta)} \tag{2}$$

Since grating loabes have the same array gains as mainlobe,

$$|F(\theta_g)| = |\frac{1}{N}\sum_{k=1}^{N} e^{j2\pi(k-1)m\sin(\theta_g)}| = 1 \tag{3}$$

where θ_g is azimuth angle with respect to grating lobes which will lead to the confusions on DOA estimation. Therefore all integral values of m make the argument an integral multiple of 2π for all values of k. Hence, grating lobes exist at:

$$sin(\theta_g) = \pm\frac{i}{m} = \pm i\frac{\lambda}{d}, i = 1, \ldots, m \tag{4}$$

Take $d = 10\lambda$ as an example, grating lobes exist at $\sin(\pm 5.73^\circ) = \pm 0.1$, $\sin(\pm 11.53^\circ) = \pm 0.2$, ..., and $\sin(\pm 90^\circ) = \pm 1$ as shown in Figure 2. The field of view (FOV) of array is drastically reduced from 180° to 5.73°. Since grating lobes will significantly degrade the array performance, it is desirable to design a novel grating lobes-free architecture for distributed sensor system with arbitrary element spacing.

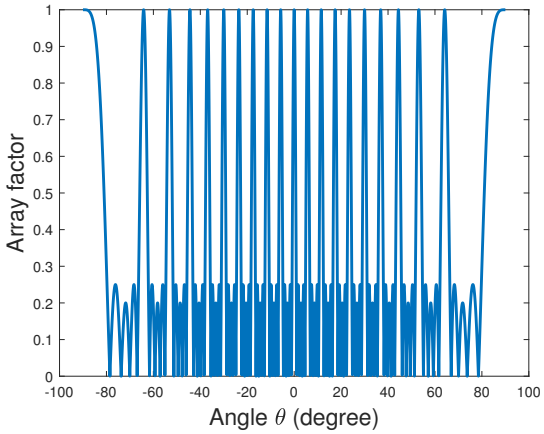

Figure 2. Grating lobes of distributed sensor system when $N = 5$ and $d = 10\lambda$.

It can be observed from (4) that the spacing between grating lobes is λ/d. Thus a value of d slightly smaller than one wavelength ensures no large, spurious response of the array to energy arriving from any direction. However, the FOV is $\theta_0 \in [-\pi/2, \pi/2]$. To avoid grating lobes at these extreme steering angles, the lobe separation should be two or greater. For a traditional phased-array radar, the condition for avoidance of all grating lobes under all conditions of beam-steering is Anderson [37]:

$$\frac{\lambda}{d} = \frac{c}{df} \geq 2 \tag{5}$$

where c is the speed of the light and f is the carrier frequency. The element spacing must satisfy the relation:

$$d \leq \frac{\lambda}{2} = \frac{c}{2f} \tag{6}$$

3. The Proposed Grating Lobes-Free Architecture

As discussed in Section 2, current array radar system is based on single carrier frequency and element spacing d should be smaller than $\lambda/2$ to avoid the grating lobes. The constraint $d \leq \lambda/2$ greatly limits the application of array radar system.

Based on dual carrier frequency measurements, this paper designs a novel grating lobes-free architecture for a distributed sensor system to obtain the unambiguous DOA estimate in whole FOV $[-\pi/2, \pi/2]$.

The proposed architecture operates at two carrier frequencies f_1 and f_2 which are generated by a local oscillator (LO) as shown in Figure 3. Both two carrier frequencies are combined and transmitted simultaneously. For each receiving sensor, there are two receive channels corresponding to two carrier frequencies f_1 and f_2. Frequency-domain filter and time-division technique are used for synchronous and asynchronous modes to separate f_1 and f_2. A more detailed discussion on those two modes will be presented in the Remark 2 of this paper. For a grating lobes-free architecture, it is proved in (6) and (16) that the element spacing d is inversely proportional to f_1 and $f_2 - f_1$ for single frequency system and the proposed dual frequency system, respectively. Obviously, the lower f_1 and $f_2 - f_1$ will result in the larger d. Since $f_2 - f_1$ is much less than f_1 and the choice of $f_2 - f_1$ is more flexible, the proposed method can provide an unambiguous DOA estimate in the whole FOV for arbitrary element spacing.

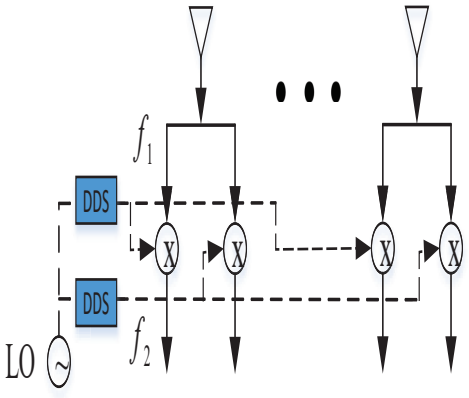

Figure 3. The proposed grating lobes-free architecture.

It should be noted that both f_1 and f_2 are narrow-band pulse signals. Both range estimates in our system and traditional phased-array radar are all based on pulse compression technology. Compared with the traditional phased-array radar based on single carrier frequency, the main contribution of the proposed architecture is to use the dual frequency measurements to design a grating lobes-free distributed sensor system with arbitrary element spacing.

Assuming that ϕ_{k1} and ϕ_{k2} are the phases corresponding to two carrier frequencies at the kth receiving sensor and r_k is the true distance between the target and the kth sensor, the relation between ϕ_{kj} and r_k can be written as

$$\phi_{kj} = \phi_0 - \frac{2\pi f_j r_k}{c} = \phi_0 - \frac{2\pi r_k}{\lambda_j} \tag{7}$$

where ϕ_0 is the initial phase of the signal, λ_1 and λ_2 are the wavelengths of the two frequencies f_1 and f_2, respectively. Noting that $r_k \approx r - x_k \sin(\theta_0)$ in a far-field situation where r is the distance between target and the array center. Substituting it into (7), gives:

$$\phi_{kj} = \phi_0 - \frac{2\pi f_j}{c}(r - x_k \sin(\theta_0)) \tag{8}$$

The phase difference $\phi_{k2} - \phi_{k1}$ is:

$$\phi_{k2} - \phi_{k1} = \frac{2\pi(x_k \sin(\theta_0) - r)(f_2 - f_1)}{c} \tag{9}$$

Equation (9) shows that the initial phase ψ_k in (10) can be used in the proposed dual frequencies architecture to synchronize the carriers of the kth sensor for forming a beam in the desired direction.

$$\psi_k = -\frac{2\pi(f_2 - f_1)x_k \sin(\theta_0)}{c} \tag{10}$$

Using the same definition (1) used in single frequency system, the array factor of the proposed architecture becomes:

$$\begin{aligned} F(\theta) &= \frac{1}{N}\sum_{k=1}^{N} e^{j\psi_k} e^{j2\pi(x_k \sin(\theta) - r)(f_2 - f_1)/c} \\ &= e^{-j2\pi r(f_2 - f_1)/c} \times \\ &\frac{1}{N}\sum_{k=1}^{N} e^{j2\pi(f_2 - f_1)x_k(\sin(\theta) - \sin(\theta_0))/c} \end{aligned} \tag{11}$$

Since the first term of (11) will not affect the amplitude of $F(\theta)$, (11) can be rewritten as:

$$F(\theta) = \frac{1}{N}\sum_{k=1}^{N} e^{j2\pi(f_2 - f_1)x_k(\sin(\theta) - \sin(\theta_0))/c} \tag{12}$$

Considering a general case with $\theta_0 = 0$, (12) can be simplified as:

$$F(\theta) = \frac{1}{N}\sum_{k=1}^{N} e^{j2\pi(f_2 - f_1)x_k \sin(\theta)/c} \tag{13}$$

Let $F(\theta_g) = 1$, grating lobes of the proposed method exist at:

$$sin(\theta_g) = \pm\frac{ic}{d(f_2 - f_1)} = \pm\frac{i\lambda_1\lambda_2}{d(\lambda_2 - \lambda_1)} \tag{14}$$

Like (5), the condition for avoidance of all grating lobes for the proposed architecture is:

$$\frac{c}{d(f_2 - f_1)} = \frac{\lambda_1\lambda_2}{d(\lambda_2 - \lambda_1)} \geq 2 \tag{15}$$

and the above equation shows that the element spacing must satisfy the relation:

$$d \leq \frac{\lambda_1\lambda_2}{2(\lambda_2 - \lambda_1)} = \frac{c}{2(f_2 - f_1)} \tag{16}$$

Remark 1. *Compared (6) with (16), the element spacing d of the traditional phased-array radar totally depends on the carrier frequency f, whereas the frequency separation $f_2 - f_1$ determines the element spacing d in the proposed method. Since many factors such as spectrum interference and antenna size will affect the selection of f, reducing f to increase d is not easy. Even if the traditional radar chooses a low carrier frequency such as metric wave $f = 300$ Mhz, the maximum element spacing without grating lobes is only 0.5 m. Compared with single carrier frequency, the choice of frequency separation $f_2 - f_1$ is much more flexible. Proper selection of $f_2 - f_1$ can provide an unambiguous DOA estimate in the whole FOV $[-\pi/2, \pi/2]$ for arbitrary element spacing d.*

Figure 4 shows the element spacing d versus different frequency separations for the case of grating lobes-free design. In the figure, $f_2 - f_1$ varies from 1 Mhz to 300 Mhz. It is observed from Figure 4 that the element spacing increases as the frequency separation

becomes small. For $f_2 - f_1 = 1$ Mhz, $d = 150$ m which can meet the most requirements on distributed range of distributed sensor system.

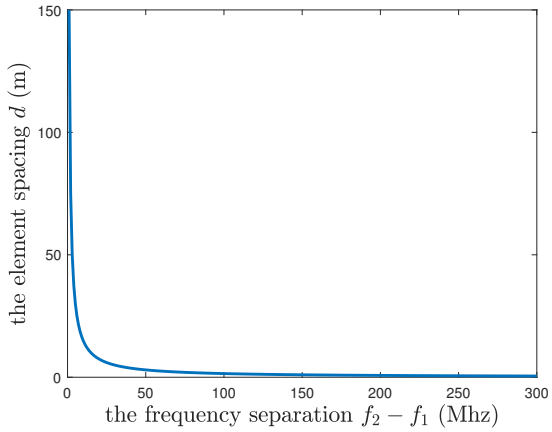

Figure 4. The element spacing d versus different frequency separations $f_2 - f_1$ for the case of grating lobes-free design.

Array factor comparisons between the proposed architecture based on dual carrier frequencies and the traditional method designed for single carrier frequency is shown in Figure 5. In this figure, $f = 3$ Ghz, $d = 10\lambda$, $N = 21$, and $f_2 - f_1 = 150$ Mhz. It can be seen from the figure that the proposed method can provide the unambiguous DOA estimate in the whole FOV $[-\pi/2, \pi/2]$, whereas the traditional method has many grating lobes and the FOV of the traditional method is only 5.73°.

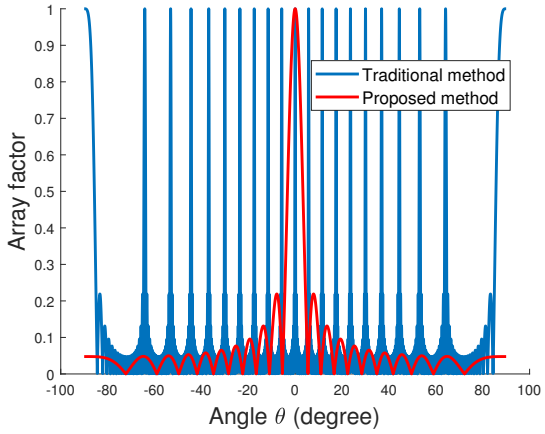

Figure 5. Array factor comparisons between the proposed method and traditional method.

Remark 2. *There are synchronous and asynchronous modes to transmit and separate f_1 and f_2. Noting that both two signals have the same bandwidth B. For the case of $f_2 - f_1 > B$, f_1 and f_2 are transmitted simultaneously and analog or digital frequency-domain filter can be used in the receive channel to separate the two signals. For the case of small frequency separation such as $f_2 - f_1 < B$, the frequency bands of f_1 and f_2 may overlap. The stepped-frequency technique can be used to distinguish the signals at f_1 and f_2 based on time-division method as shown in Figure 6.*

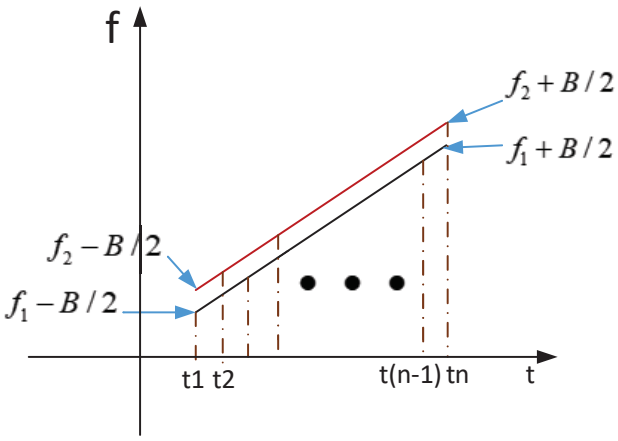

Figure 6. Asynchronous mode using stepped-frequency technique.

It should be noted that asynchronous mode will bring an additional phase perturbation κ due to the movement of target between the time gap $t_i - t_{i-1}$.

$$\kappa = -2\pi f_2 v(t_i - t_{i-1})/c \tag{17}$$

where v is the radial velocity between the array and target. According to (17), the switching time $t_i - t_{i-1}$ must meet the following constraint:

$$t_i - t_{i-1} \leq |c\kappa/(2\pi f_2 v)| \tag{18}$$

Diverse system design requirements will result in different switching time $t_i - t_{i-1}$. For example, $t_i - t_{i-1} \leq 4.62$ µs when $f_2 = 3$ Ghz, $v = 300$ m/s, and $\kappa = 5°$.

From (13), the far-field beampattern of the proposed architecture can be written as:

$$\begin{aligned} P(\theta) = |F(\theta)|^2 = F(\theta)F(\theta)^* = \frac{1}{N} + \\ \frac{1}{N^2}\sum_{i=1}^{N}\sum_{j=1,i\neq j}^{N} e^{j2\pi(f_2-f_1)(x_i-x_j)\sin(\theta)/c} \end{aligned} \tag{19}$$

Since the horizontal axis of the kth sensor x_k is uniformly distributed in $[-L/2, L/2]$, the performance of (13) and (19) can be evaluated by the average array factor and beampattern. The average array factor can be calculated as the average of (19):

$$\begin{aligned} F_{av}(\theta) = E[F(\theta)] &= \frac{1}{N}\sum_{k=1}^{N} E\left[e^{j2\pi(f_2-f_1)x_k\sin(\theta)/c}\right] \\ &= \frac{1}{N}\sum_{k=1}^{N}\frac{1}{L}\int_{-\frac{L}{2}}^{+\frac{L}{2}} e^{j2\pi(f_2-f_1)x_k\sin(\theta)/c}dx_k \\ &= \frac{\sin(\pi(f_2-f_1)L\sin(\theta)/c)}{\pi(f_2-f_1)L\sin(\theta)/c} \end{aligned} \tag{20}$$

The average far-field beampattern of the proposed architecture is written as the square of (20):

$$\begin{aligned} P_{av}(\theta) &= |F_{av}(\theta)|^2 \\ &= \left(\frac{\sin(\pi(f_2-f_1)L\sin(\theta)/c)}{\pi(f_2-f_1)L\sin(\theta)/c}\right)^2 \end{aligned} \tag{21}$$

Considering a grating lobes-free array satisfying (16) and setting $L = (N-1)d$, the average far-field beampattern (21) becomes:

$$P_{av}(\theta) = \left(\frac{\sin(\pi(N-1)\sin(\theta)/2)}{\pi(N-1)\sin(\theta)/2} \right)^2 \tag{22}$$

Figure 7 shows beampattern comparisons between (19) and (22) when $N = 16, 32, 64$. It can be observed that the average beampattern (22) matches well with the far-field beampattern (19) for different N which verifies the effectiveness of the average beampattern (22). Compared (19) and (22), the average beampattern provides a clearer and simpler expression. This can help us further analyze the array properties.

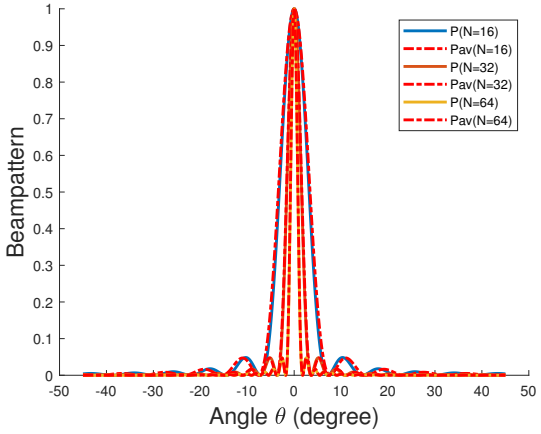

Figure 7. Beampattern comparisons for different N.

4. Properties of the Proposed Average Beampattern

The characteristics of the proposed average beampattern (22) are provided in this section.

4.1. Three dB Beamwidth

Three dB beamwidth is defined as the width of the main lobe between points 3 dB below the peak. This indicator is very important in the array radar design. Since the smaller 3 dB beamwidth will lead to the higher angle resolution, array design usually pursues the sharp mainbeam property. Nevertheless, the large 3 dB beamwidth may increase scanning area and reduce sweep time. Designing a proper 3 dB beamwidth should be based on the actual application demands. The half-width of the main lobe denoted θ^{3dB_half} as the angle θ should satisfy:

$$P_{av}(\theta^{3dB\_half}) = \frac{1}{2} \tag{23}$$

Obviously, (23) is a nonlinear equation. Using the numerical method to calculate (21), (23) holds when $\pi(f_2 - f_1)L\sin(\theta)/c = 1.39$. Noting that $\sin(\theta) \approx \theta$ for the case of small θ such as $\theta \leq 20^\circ$. Therefore,

$$\theta^{3dB\_half} \approx \frac{0.4425c}{L(f_2 - f_1)} \tag{24}$$

The 3 dB width is obtained from (24):

$$\theta^{3dB} = 2 \times \theta^{3dB\_half} \approx \frac{0.885c}{L(f_2 - f_1)} \tag{25}$$

Three dB width comparisons between the proposed and traditional methods are provided in the following Propositions. Two cases are considered in the comparisons. The first one is based on grating lobes-free design where both methods have the unambiguous DOA estimate in whole FOV $[-\pi/2, \pi/2]$. For a grating lobes-free design, the element

spacing d_p of the proposed architecture and d_t of the traditional phased-array with single carrier frequency should satisfy (16) and (6), respectively. Thus,

$$d_p = c/(2(f_2 - f_1)), d_t = c/(2f) \tag{26}$$

Another case assumes that both method have the same array aperture L and the number of sensors N.

Proposition 1. *In a grating lobes-free array, the proposed architecture has the same 3 dB beamwidth as the traditional phased-array with single carrier frequency.*

$$\theta_P^{3dB} = \theta_T^{3dB} = 1.77/(N-1) \tag{27}$$

where θ_P^{3dB} and θ_T^{3dB} are the 3 dB beamwidths of the proposed architecture and the traditional phased-array, respectively.

Meanwhile the relation of the array apertures between the proposed method L_p and traditional phased-array radar L_t is that:

$$\frac{L_p}{L_t} = \frac{d_p}{d_t} = \frac{f}{f_2 - f_1} \tag{28}$$

where d_p and d_t are the element spacing of the proposed method and the phased-array radar, respectively.

Proof. For a ULA, the array apertures can be calculated as:

$$L_p = (N-1)d_p, L_t = (N-1)d_t \tag{29}$$

(28) is easily proved from (26) and (29). Substituting (26) and (29) into (25), gives $\theta_P^{3dB} = 1.77/(N-1)$. For a phased-array with single carrier frequency, the 3 dB beamwidth is Anderson [37]:

$$\theta_T^{3dB} = 0.885\lambda/L_t \tag{30}$$

Substituting (26) and (29) into θ_T^{3dB}, gives $\theta_T^{3dB} = 1.77/(N-1)$. Hence, Proposition 1 holds. □

Remark 3. *Proposition 1 shows that the 3 dB beamwidths of both methods totally depend on the number of sensors in a grating lobes-free array. This means that increasing the number of sensors is an effective method to obtain the more sharp mainbeam property. Although both methods have the same 3 dB beamwidth for a grating lobes-free array, the element spacing of the proposed method is $f/(f_2 - f_1)$ times that of phased-array radar. Generally, a carrier frequency f is far greater than the frequency separation $f_2 - f_1$. For example, $f/(f_2 - f_1) = 300$ when $f = 3$ Ghz and $f_2 - f_1 = 10$ Mhz. Compared with the traditional method with single carrier frequency, the proposed method can provide the same angle resolution and a much larger distributed area in a grating lobes-free array. For the proposed grating lobes-free architecture, the element spacing d increases from 0.5 m to 150 m as the frequency separation $f_2 - f_1$ reduces from 300 Mhz to 1 Mhz as shown in Figure 4.*

Proposition 2. *In the case with the same array aperture L and the number of sensors N, the traditional method has the higher angle resolution:*

$$\frac{\theta_P^{3dB}}{\theta_T^{3dB}} = \frac{f}{f_2 - f_1} \gg 1 \tag{31}$$

but the narrower FOV:

$$\frac{FOV_P}{FOV_T} = \frac{f}{f_2 - f_1} \gg 1 \tag{32}$$

Proof. Dividing (25) by (30), (31) holds. In the case with grating lobes, FOV is equal to the gap of grating lobes. Thus, it can be obtained from (4) and (14) that:

$$FOV_P = \frac{c}{d(f_2 - f_1)} \tag{33}$$

$$FOV_T = \frac{c}{df} \tag{34}$$

Dividing (33) by (34), (32) holds. □

Remark 4. *Proposition 2 shows that the angle resolution depends on the array aperture and carrier frequencies. With the same array aperture, the the traditional method can provide the higher angle resolution but the narrower FOV. Both ratios between the proposed and traditional methods for angle resolution and FOV are the same $f/(f_2 - f_1)$. With the limited sensors, high angle resolution and large FOV can not be obtained at the same time. Considering a general case with $f = 3$ Ghz, $f_2 - f_1 = 10$ Mhz, $L = 180$ m, and $N = 10$, we can calculate from (25), (30), (33), and (34) that $\theta_P^{3dB} = 8.45^\circ$, $FOV_P = 85.94^\circ$, $\theta_T^{3dB} = 0.0282^\circ$, $FOV_T = 0.2865^\circ$. Although the traditional method provides much sharp mainlobe, the FOV is only 0.2865° which is impossible to be used in a practical system with such small FOV. The proposed method can struck a good balance with the angle resolution and FOV for a distributed sensor system with large array aperture.*

4.2. Peak and Zero Points of the Sidelobe

Sidelobe property is another important indicator to evaluate the array performance. Small sidelobe will improve detection capability and suppress interference. It is observed from (21) that the ith peak of the sidelobe appears around $\pi(f_2 - f_1)L\sin(\theta)/c \approx (i + 0.5)\pi, i = 1, 2, \cdots$, and its corresponding value becomes:

$$P_{av}(\theta_i^{peak}) \sim \left(\frac{1}{\left(i + \frac{1}{2}\right)\pi}\right)^2 \tag{35}$$

Considering a grating lobes-free design which satisfies (16) and $L = (N-1)d$, the ith peak and ith zero positions can be expressed asymptotically as:

$$\theta_i^{peak} \sim \arcsin\left(\frac{2(i + 0.5)}{N - 1}\right) \tag{36}$$

$$\theta_i^{zero} \sim \arcsin\left(\frac{2i}{N - 1}\right) \tag{37}$$

The peak sidelobe ratio can be calculated as:

$$\begin{aligned} PSR &= \frac{P_{av}(\theta_0)}{P_{av}(\theta_1^{peak})} = 1/\left(\frac{1}{\left(1 + \frac{1}{2}\right)\pi}\right)^2 \\ &= 13.47dB \end{aligned} \tag{38}$$

Since the value of the ith peak of the sidelobe is a constant as shown in (36), it is impossible to bring down the peak value of the sidelobe and the only way one can avoid high peaks in the sidelobe region is to increase N such that most of the major peaks are relatively concentrated around the main lobe. Equation (38) shows that the proposed method will not increase the maximum sidelobe level. In contrast, current sensor position diversity techniques used for grating lobes suppression greatly enhance the sidelobe level specially for wide area distributed system.

Figure 8 shows the peak and zero points of the sidelobe which are calculated by (36) and (37) for $N = 8$ and $N = 16$. It can be seen from the figure that both (36) and (37) can

provide a good position estimate for peak and zero points. In addition, all of the average beampatterns (22) for $N = 8$ and $N = 16$ have the same first peak value which is consistent with (38).

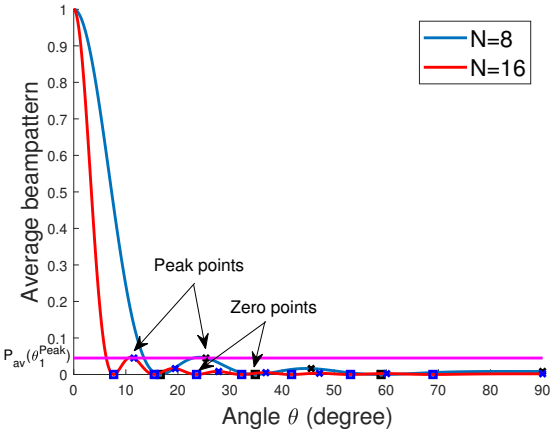

Figure 8. Peak and Zero Points of the Sidelobe.

4.3. Three dB Sidelobe Region

As shown in Figure 9, the 3dB sidelobe region is used to show the region within which neighboring sidelobe peak in the beampattern exceeds 3dB above $1/N$ Ochiai et al. [36]. Let i_0 denotes the minimum index of the peak position such that the corresponding peak value satisfies this 3 dB condition. From (22), we have:

$$P_{av}(\theta_i^{peak}) \sim \left(\frac{1}{\left(i + \frac{1}{2}\right)\pi} \right)^2 \leq \frac{2}{N} \tag{39}$$

From (39), i_0 can be bounded by:

$$i_0 \geq \frac{1}{\pi\sqrt{2/N}} - \frac{1}{2} \tag{40}$$

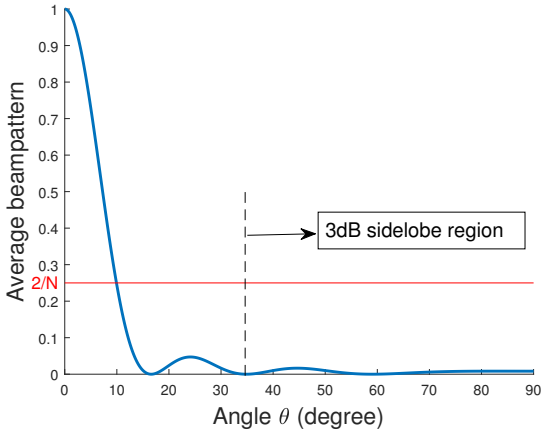

Figure 9. Definition of 3dB sidelobe region.

Substituting $i_0 + 1$ into (37), $\theta_{i_0+1}^{zero}$ can be obtained. $\theta_{i_0+1}^{zero}$ denotes the angle corresponding to the zero point next to the i_0th peak sidelobe. Thus, 3dB sidelobe region is defined as the range between the angle $\theta_{i_0+1}^{zero}$ and $\pi/2$ as follows:

$$S_{3dB} = \left\{ \theta \,|\, \theta_{i_0+1}^{zero} \leq \theta \leq \pi/2 \right\} \tag{41}$$

The 3 dB sidelobe region describes the region that the beampattern of (22) sampled at $\theta \in S_{3dB}$ becomes small. In this region, the sidelobes with high peaks are less probable. Large 3 dB sidelobe region may be more popular in a array design because it can reduce interference among various targets in different directions. Figure 10 shows the 3 dB sidelobe region versus different numbers of sensors N. It can be obtained from the figure that increasing the number of sensors N can effectively enlarge 3 dB sidelobe region.

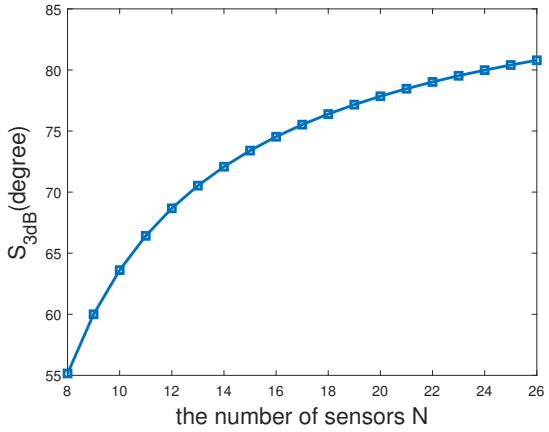

Figure 10. 3 dB sidelobe region versus different N.

4.4. Average Directivity

The average directivity is used to describe how much radiated energy the mainlobe contains, which is defined as:

$$D_{av} = \frac{\int_{-\frac{\theta^{3dB}}{2}}^{\frac{\theta^{3dB}}{2}} P_{av}(\theta)d\theta}{\int_{-\frac{\pi}{2}}^{\frac{\pi}{2}} P_{av}(\theta)d\theta} \tag{42}$$

The numerator in the above equation is the radiated energy of the mainlobe while the denominator contains the radiated energy of the whole FOV.

Substituting (22) and (27) into (42), the average directivity becomes:

$$D_{av} = \frac{\int_{-\frac{0.885}{N-1}}^{\frac{0.885}{N-1}} \left(\frac{\sin(\pi(N-1)\sin(\theta)/2)}{\pi(N-1)\sin(\theta)/2}\right)^2 d\theta}{\int_{-\frac{\pi}{2}}^{\frac{\pi}{2}} \left(\frac{\sin(\pi(N-1)\sin(\theta)/2)}{\pi(N-1)\sin(\theta)/2}\right)^2 d\theta} \tag{43}$$

Since it is hard to obtain a analytical solution for the above equation, numerical integration method such as Matlab function "integral" can be used to solve (43). Figure 11 shows the average directivity comparisons when $N = 16, 32, 64, 128, 256$. It can be observed that the average directivity increases as N increases and it will asymptotically attain 0.7217. Figure 11 also implies that the differences among the average directivities for various N are very small. For example, there is only 0.46% difference between the average directivities for $N = 16$ and $N = 256$.

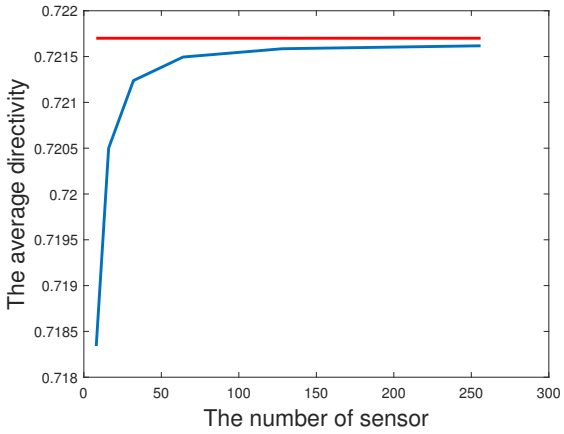

Figure 11. Average directivity comparisions for different N.

5. Performance of the Proposed Architecture with Imperfect System Synchronization

As discussed above, the performance of the proposed architecture with perfect synchronization has been evaluated in Section 4. For a phased array radar, all antennas share the same LO and clock source. Moreover, the information on antenna position for phased array radar is exact. Therefore, system synchronization error is not a main factor affecting the system performance. Due to the independent LO and clock source in each sensor, it is almost impossible for a distributed sensor system system to achieve a perfect system synchronization in a practical system. This section analyzes the effects of the phase ambiguities in terms of the average combining efficiency. The phase ambiguities considered in this paper are caused by the imperfect system synchronization including synchronization errors on position, carrier frequency, and sampling time. Both the average combining efficiencies of the traditional distributed sensor system based on single carrier frequency and the proposed architecture are first derived for the case with imperfect phase. Subsequently, comparisons between the two ways are provided in the end of this section.

Phase offset is mainly caused by the shift of carrier frequency, position estimate, and sampling time. This section provides a detail analysis for the effects of these errors. Because of the large distributed area, every sensor has the independent LO, position, and clock source. For sensor k, Δt_k and Δx_k are assumed to be the synchronization errors on sampling time and sensor position, respectively. Let f_0 is the eigenfrequency of a LO and Δf_k is the frequency shift of f_0 in sensor k. Due to the central-limit theorem, Δt_k, Δx_k, and Δf_k can be reasonably modeled as Gaussian random variables with zero mean and standard variances (stds) σ_t, σ_x, and σ_f, respectively. This paper assumes that all of Δt_k, Δx_k, and Δf_k are short stationary process. This implies that these values remain unchanged for at least one pulse period. The assumption is reasonable since one pulse period is usually very short such as ns or us level.

5.1. Average Combining Efficiency for the Proposed Architecture

Since the receive channels mix the received signal down to IF-frequency "Zero" and analog to digital converter (ADC) is directly applied to the baseband signal, the phase offset caused by Δt_k for frequency f_j in sensor k can be modeled as:

$$\varphi_{tkj} = 2\pi B \Delta t_k \tag{44}$$

where B is the bandwidth of the baseband signal. Because the phase difference (9) between the two carrier frequencies in a sensor is used in the proposed method, φ_{tkj} will be finally eliminated. This means that the proposed method has no need of the strict time synchronization required by traditional array radar. The detail discussion will be given later.

Since both f_1 and f_2 are driven by the same LO in a sensor, the shift of two carrier frequencies in sensor k can be modeled as:

$$\Delta f_{kj} = \frac{f_j}{f_0}\Delta f_k, j = 1, 2 \tag{45}$$

In the case with the phase offset, the initial phase of sensor k in (10) can be rewritten as:

$$\widetilde{\psi}_k = -\frac{2\pi(f_2 - f_1)x_k \sin(\theta_0)}{c} + \varphi_k \tag{46}$$

where φ_k is the phase offset caused by synchronization errors. As discussed in (44), Δt_k will be finally eliminated in the proposed method. Thus, φ_k is mainly caused by the shift of sensor position and frequency in sensor k. Using the perturbation approach on (10), φ_k can be calculated as:

$$\begin{aligned}\varphi_k = &-\frac{2\pi(f_2 - f_1)/f_0 x_k \sin(\theta_0)}{c}\Delta f_k \\ &-\frac{2\pi(f_2 - f_1)\sin(\theta_0)}{c}\Delta x_k\end{aligned} \tag{47}$$

Note that both Δf_k and Δx_k are subject to Gaussian distribution. They have zero mean and the corresponding stds are σ_f and σ_x, respectively. Obviously, φ_k is also a zero mean Gaussian variable with the following variance:

$$\sigma_{\varphi_k}^2 = \left(\frac{2\pi(f_2 - f_1)\sin(\theta_0)}{c}\right)^2\left(\left(\frac{x_k}{f_0}\sigma_f\right)^2 + \sigma_x^2\right) \tag{48}$$

It can be seen from (48) that $\sigma_{\varphi_k}^2$ depends on the the azimuth angle θ_0, sensor position x_k, frequency shift σ_f, and location error σ_x. Even with the same σ_f and σ_x, every sensor has the different $\sigma_{\varphi_k}^2$ due to θ_0 and x_k.

Substituting (46) into (12), the far-field array factor with imperfect phase becomes:

$$\widetilde{F}(\theta) = \frac{1}{N}\sum_{k=1}^{N} e^{j2\pi(f_2 - f_1)x_k(\sin(\theta) - \sin(\theta_0))/c} e^{j\varphi_k} \tag{49}$$

The combining efficiency is defined as the expected value of the ratio of the mainlobe amplitude to the design value:

$$A_\varphi = E\left[\frac{\widetilde{F}(\theta_0)}{F(\theta_0)}\right] \tag{50}$$

Substituting $\theta = \theta_0$ into (12) and (49), gives:

$$F(\theta_0) = \frac{1}{N}\sum_{k=1}^{N} e^{j2\pi(f_2 - f_1)x_k(\sin(\theta_0) - \sin(\theta_0))/c} = 1 \tag{51}$$

$$\widetilde{F}(\theta_0) = \frac{1}{N}\sum_{k=1}^{N} e^{j\varphi_k} \tag{52}$$

Substituting (51) and (52) into (50), gives:

$$A_\varphi = E\left[\frac{1}{N}\sum_{k=1}^{N} e^{j\varphi_k}\right] = \frac{1}{N}\sum_{k=1}^{N} E\left[e^{j\varphi_k}\right] \tag{53}$$

Obviously, $A_\varphi = 1$ for the case with perfect synchronization $\varphi_k = 0$. Note that

$$\begin{aligned} & E\left[e^{j\varphi_k}\right] \\ &= \int_{-\infty}^{+\infty} e^{j\varphi_k} \frac{1}{\sqrt{2\pi}\sigma_{\varphi_k}} e^{-\varphi_k^2/\left(2\sigma_{\varphi_k}^2\right)} d\varphi_k \\ &= e^{-\sigma_{\varphi_k}^2/2} \end{aligned} \tag{54}$$

Substituting (54) into (53), gives:

$$A_\varphi = \frac{1}{N}\sum_{k=1}^{N} e^{-\sigma_{\varphi_k}^2/2} \tag{55}$$

As discussed in (48), σ_{φ_k} has different values for various θ_0 and x_k. Thus, the average combining efficiency is defined as the average of (55) to evaluate the average performance of the distributed array system:

$$\bar{A_\varphi} = E\left[A_\varphi\right] = \frac{1}{N}\sum_{k=1}^{N} E\left[e^{-\sigma_{\varphi_k}^2/2}\right] \tag{56}$$

Obviously, (56) has not closed-form solution due to the unknown distribution of $\sigma_{\varphi_k}^2$. The further approximation should be developed for performance analysis. With a sufficiently large N, the expected mean can be replaced with the sample mean and the average combining efficiency (56) is approximated as:

$$\bar{A_\varphi} \approx \frac{1}{N}\sum_{k=1}^{N} e^{-E\left[\sigma_{\varphi_k}^2\right]/2} \tag{57}$$

From (48), the average variance is solved as:

$$\begin{aligned} \sigma_\varphi^2 &= E\left[\sigma_{\varphi_k}^2\right] \\ &= \left(\frac{2\pi(f_2 - f_1)\sigma_x}{c}\right)^2 E\left[\sin^2(\theta_0)\right] \\ &+ \left(\frac{2\pi(f_2 - f_1)\sigma_f}{cf_0}\right)^2 E\left[\sin^2(\theta_0)x_k^2\right] \end{aligned} \tag{58}$$

Assuming that the target is uniformly distributed in the whole FOV $[-\pi/2, \pi/2]$, we have:

$$E\left[\sin^2(\theta_0)\right] = \int_{-\frac{\pi}{2}}^{+\frac{\pi}{2}} \frac{\sin^2(\theta_0)}{\pi} d\theta_0 = \frac{1}{2} \tag{59}$$

Since θ_0 and x_k are independent, $E\left[\sin^2(\theta_0)x_k^2\right]$ can be expressed as:

$$E\left[\sin^2(\theta_0)x_k^2\right] = E\left[\sin^2(\theta_0)\right] E\left[x_k^2\right] \tag{60}$$

Note that x_k is uniformly distributed in $[-L/2, L/2]$, $E\left[x_k^2\right]$ is computed as:

$$E\left[x_k^2\right] = \int_{-\frac{L}{2}}^{+\frac{L}{2}} \frac{x_k^2}{L} dx_k = \frac{x_k^3}{3L}\Big|_{-\frac{L}{2}}^{+\frac{L}{2}} = \frac{L^2}{12} \tag{61}$$

Substituting (59)~(61) into (58), σ_{φ}^2 in (58) becomes:

$$\begin{aligned}\sigma_{\varphi}^2 &= E\left[\sigma_{\varphi_k}^2\right] \\ &= \left(\frac{2\pi(f_2 - f_1)}{c}\right)^2 \left(\frac{\sigma_x^2}{2} + \frac{L^2}{24}\left(\frac{\sigma_f}{f_0}\right)^2\right)\end{aligned} \tag{62}$$

Substituting (62) into (57), the average combining efficiency is

$$\bar{A_{\varphi}} \approx e^{-\sigma_{\varphi}^2/2} = \bar{A_{\varphi_x}} \bar{A}_{\varphi_f} \tag{63}$$

with

$$\begin{aligned}\bar{A_{\varphi_x}} &= e^{-\left(\frac{\pi(f_2-f_1)}{c}\right)^2 \sigma_x^2} \\ \bar{A}_{\varphi_f} &= e^{-\left(\frac{\pi(f_2-f_1)}{c}\right)^2 \left(\frac{L^2}{12}\left(\frac{\sigma_f}{f_0}\right)^2\right)}\end{aligned} \tag{64}$$

where $\bar{A_{\varphi_x}}$ and $\bar{A_{\varphi_f}}$ describes the performance degradation caused by the shift of the position and LO, respectively.

Figure 12 shows the comparisons between the actual combining efficiency and the theoretical combining efficiency. The former is calculated by (53) while the proposed average combining efficiency (63) is used to compute the latter. In the figure, $f_2 - f_1 = 300$ Mhz, $\sigma_x = 0.01$ m, $\sigma_f = 100$ khz, N varies from 5 to 50, and the actual combining efficiency (53) is obtained from the average of 10,000 independent runs.

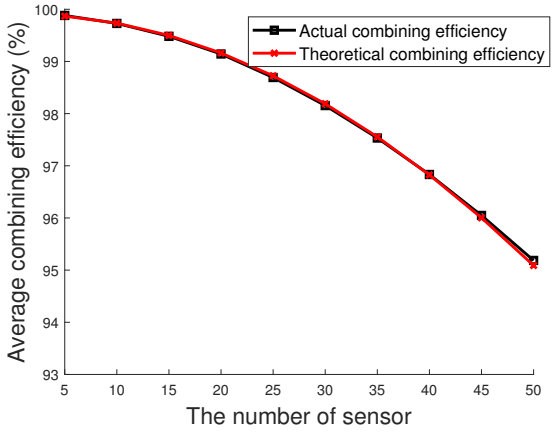

Figure 12. Combining efficiency comparisons for different N.

Although the actual combining efficiency can be computed by using (53), it is very hard to use (53) for performance analysis. This is caused by the non-closed-form solution of (53) due to the unknown distribution of phase offset. For the better theoretical analysis, the proposed average combining efficiency (63) with closed-form solution is developed to describe the actual combining efficiency (53). It can be observed from Figure 12 that the proposed average combining efficiency can well match the actual combining efficiency (53) which proves the effectiveness of the proposed average combining efficiency (63). In other words, the proposed average combining efficiency (63) can be used to evaluate the performance of a real distributed sensor system. Moreover, various affecting factors of the combining efficiency can be analyzed using (63). Equation (63) shows that the combining efficiency is inversely proportional to frequency separation $f_2 - f_1$ and synchronization errors (σ_x and σ_f).

Considering a grating lobes-free design $L_p = (N-1)d_p$ and $d_p = c/(2(f_2 - f_1))$, (64) becomes:

$$\begin{aligned} \bar{A_{\varphi_x}} &= e^{-\left(\frac{\pi(N-1)}{2}\right)^2\left(\frac{\sigma_x}{L_p}\right)^2} \\ \bar{A}_{\varphi_f} &= e^{-\left(\frac{\pi(N-1)}{2}\right)^2\left(\frac{1}{12}\left(\frac{\sigma_f}{f_0}\right)^2\right)} \end{aligned} \tag{65}$$

where L_p and d_p are the array aperture and element spacing of the proposed method, respectively.

Figure 13 shows the average combining efficiency $\bar{A_\varphi}$ versus different stds of phase offset σ_φ for $N = 20$. As σ_φ increases, the average combining efficiency $\bar{A_\varphi}$ becomes small which means the performance of array is deteriorating. The average combining efficiency is a powerful tool to determine the requirement of system synchronization which is presented in the following example. For an acceptable tolerance such as $\bar{A_\varphi} = 90\%$, the std of phase offset σ_φ should be less than 26° as shown in Figure 13. Phase offset is the total phase error caused by the position and frequency errors σ_x and σ_f. Further decomposition is required for system design. Considering a system with system parameters $f_2 - f_1 = 100$ Mhz, $f_0 = 10$ Mhz and $\sigma_\varphi < 26°$, the requirements of system synchronization ($\sigma_x \leq 0.3$ m and $\sigma_f \leq 330$ khz) can be obtained using (63). In other words, σ_x and σ_f must be less than 0.3 m and 330 khz to make $\bar{A_\varphi} \geq 90\%$.

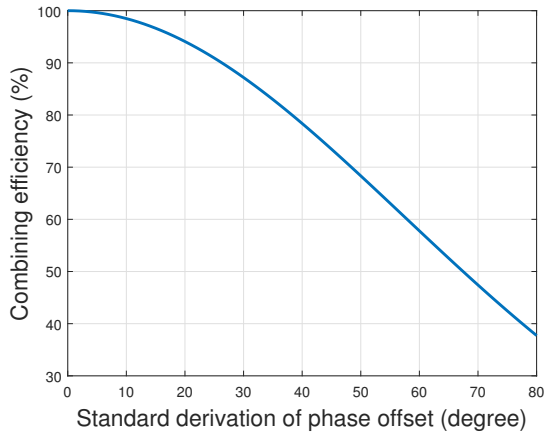

Figure 13. Combining efficiency versus different stds of phase offset.

5.2. Average Combining Efficiency for the Traditional Method

A traditional phased array system usually operates at a single carrier frequency f. It can be seen from (44) that the phase offset caused by the time synchronization error Δt_k for sensor k can be modeled as:

$$\varphi_{tk} = 2\pi B \Delta t_k \tag{66}$$

The difference with the proposed architecture is that (66) cannot be eliminated in a traditional method due to the single carrier frequency. Considering the initial phase $\psi_k = -2\pi x_k \sin(\theta_0)/\lambda$ in (1) for perfect system synchronization, ψ_k can be rewritten as follows in the case with imperfect phase:

$$\widetilde{\psi}_k = -\frac{2\pi x_k f \sin(\theta_0)}{c} + \varepsilon_k \tag{67}$$

where ε_k is the phase offset caused by synchronization errors. Using the perturbation approach, ε_k can be calculated as:

$$\begin{aligned}\varepsilon_k = &-\frac{2\pi x_k \sin(\theta_0)}{c}\frac{f}{f_0}\Delta f_k \\ &-\frac{2\pi f \sin(\theta_0)}{c}\triangle x_k + 2\pi B \Delta t_k\end{aligned} \tag{68}$$

Since all of Δf_k, $\triangle x_k$, and Δt_k are zero mean Gaussian random variables, ε_k is also subject to Gaussian distribution with zero mean and variance:

$$\sigma_{\varepsilon_k}^2 = \left(\frac{2\pi f \sin(\theta_0)}{c}\right)^2 \left(\left(\frac{x_k}{f_0}\sigma_f\right)^2 + \sigma_x^2\right) + (2\pi B \sigma_t)^2 \tag{69}$$

The average variance σ_ε^2 is:

$$\begin{aligned}\sigma_\varepsilon^2 = E\left[\sigma_{\varepsilon_k}^2\right] = (2\pi B\sigma_t)^2 + \left(\frac{2\pi f}{c}\right)^2 \times \\ \left(\left(\frac{\sigma_f}{f_0}\right)^2 E\left[\sin^2(\theta_0)\right] E\left[x_k^2\right] + \sigma_x^2 \mathrm{E}\left[\sin^2(\theta_0)\right]\right)\end{aligned} \tag{70}$$

Substituting (59)~(61) into (70), gives:

$$\sigma_\varepsilon^2 = \left(\frac{2\pi f}{c}\right)^2 \left(\left(\frac{\sigma_f}{f_0}\right)^2 \frac{L^2}{24} + \frac{\sigma_x^2}{2}\right) + (2\pi B\sigma_t)^2 \tag{71}$$

Using the similar method as (63), the average combining efficiency for the traditional method based on a single carrier frequency is derived as:

$$\bar{A}_\varepsilon \approx e^{-\sigma_\varepsilon^2/2} = \bar{A_{\varepsilon_t}} \bar{A_{\varepsilon_x}} \bar{A}_{\varepsilon_f} \tag{72}$$

where

$$\begin{aligned}\bar{A_{\varepsilon_x}} &= e^{-\left(\frac{\pi f}{c}\right)^2 \sigma_x^2} \\ \bar{A}_{\varepsilon_f} &= e^{-\left(\frac{\pi f}{c}\right)^2 \left(\frac{L^2}{12}\left(\frac{\sigma_f}{f_0}\right)^2\right)} \\ \bar{A_{\varepsilon_t}} &= e^{-(2\pi B\sigma_t)^2/2}\end{aligned} \tag{73}$$

Remark 5. *Compared (63) with (72), the phase difference (9) used in the proposed method eliminates the phase offset $2\pi B\sigma_t$ caused by time synchronization error $\triangle t_k$, whereas $\triangle t_k$ will bring the gain attenuation $\bar{A_{\varepsilon_t}}$ to a traditional method. For an ideal situation such as continuous wave radar with a fixed target, there is no need for the proposed method to synchronize sampling time. For a more general case with pulse radar and moving target, a looser requirement on the precision of time synchronization should be satisfied by the proposed method to capture the same pulse. For a pulse radar, the time bandwidth product BT is usually much larger than 1 where T is the pulse width. Roughly speaking, the requirement of time synchronization accuracy for the traditional method is BT times of that for the proposed method. This means the traditional method must have the smaller time synchronization error.*

Considering a grating lobes-free design $L_t = (N-1)d_t$ and $d_t = c/(2f)$, (73) becomes:

$$\begin{aligned} \bar{A_{\varepsilon_x}} &= e^{-\left(\frac{\pi(N-1)}{2}\right)^2\left(\frac{\sigma_x}{L_t}\right)^2} \\ \bar{A_{\varepsilon_f}} &= e^{-\left(\frac{\pi(N-1)}{2}\right)^2\left(\frac{1}{12}\left(\frac{\sigma_f}{f_0}\right)^2\right)} \\ \bar{A_{\varepsilon_t}} &= e^{-(2\pi B\sigma_t)^2/2} \end{aligned} \tag{74}$$

where L_t and d_t are the array aperture and element spacing of the array radar with single carrier frequency, respectively.

5.3. Characteristics of the Proposed Average Combining Efficiency

The characteristics of the proposed average combining efficiency are provided in the following Propositions.

Proposition 3. *With the same position estimate error σ_x, the proposed method can provide the higher combining efficiency than the traditional method based on single carrier frequency.*

$$\frac{\bar{A_{\varphi_x}}}{\bar{A_{\varepsilon_x}}} = e^{\left(\frac{\pi\sigma_x}{c}\right)^2\left(f^2-(f_2-f_1)^2\right)} \gg 1 \tag{75}$$

Proof. The above equation can be easily proved from (64) and (73).

Because single carrier frequency f is usually much larger than frequency separation $f_2 - f_1$, $\left(f^2 - (f_2 - f_1)^2\right) \gg 0$ and $\bar{A_{\varphi_x}}/\bar{A_{\varepsilon_x}} \gg 1$.

Hence, Proposition 3 holds. □

Remark 6. *Proposition 3 shows that the proposed method has the higher array combining efficiency than the traditional method in the case of the same σ_x. For example, $\bar{A_{\varphi_x}}/\bar{A_{\varepsilon_x}} = 11.79$ when $f = 3$ Ghz, $f_2 - f_1 = 10$ Mhz, and $\sigma_x = 0.05$ m. This means that the proposed method can provide 21.43 dB power gains than the single frequency system for the above system setting. Proposition 3 also implies that the traditional method has the more strict requirement on positioning error in the case of the same combining efficiency. Let $\bar{A_{\varphi_x}} = \bar{A_{\varepsilon_x}}$,*

$$\frac{\sigma_{xp}}{\sigma_{xt}} = \frac{f}{f_2 - f_1} \tag{76}$$

where σ_{xp} and σ_{xt} are the stds of sensor position errors of the proposed method and the traditional method, respectively. For $f = 3$ Ghz and $f_2 - f_1 = 10$ Mhz, $\sigma_{xp}/\sigma_{xt} = 300$. This means that the requirement on position synchronization accuracy for the traditional method is 300 times of that for the proposed method. To obtain the same combining efficiency, the requirement on the positioning error of the proposed method is $\sigma_{xp} = 6$ m, whereas the location error of the traditional method must be smaller than $\sigma_{xt} = 0.02$ m. Hence, the proposed method can greatly reduce hardware requirements.

Proposition 4. *In a grating lobes-free array, the effects on the average combining efficiency caused by the frequency shift for both methods are the same:*

$$\bar{A}_{\varepsilon_f} = \bar{A}_{\varphi_f} = e^{-\left(\frac{\pi(N-1)}{2}\right)^2\left(\frac{1}{12}\left(\frac{\sigma_f}{f_0}\right)^2\right)} \tag{77}$$

Nevertheless, the proposed method can provide the higher combining efficiency than the traditional method for the case with the same array aperture L and frequency shift σ_f:

$$\frac{\bar{A}_{\varphi_f}}{\bar{A}_{\varepsilon_f}} = e^{\left(\frac{1}{12}\left(\frac{L\pi\sigma_f}{cf_0}\right)^2\right)\left(f^2-(f_2-f_1)^2\right)} \gg 1 \tag{78}$$

Proof. From (65) and (74), (77) is proved. Dividing (64) by (73), (78) holds. □

Remark 7. *It can be concluded from Remark 5, Proposition 3, and (75) that the proposed method has the higher combining efficiency than the traditional method with the same synchronization errors on position estimate and sampling time. There are two cases for the effects of the frequency shift. For a grating lobes-free array, the effects of the frequency shift for both methods are the same. However, the proposed method can provided a much larger distributed area in a grating lobes-free array as discussed in Remark 3. For another case with the same array aperture and frequency shift, the proposed method has the higher combining efficiency.*

Finally, comparisons between the single frequency system Jayaprakasam et al. [2], Diaz et al. [3], Mudumbai et al. [4], Li and Nehorai [31], Huang et al. [34], Ahmed and Vorobyov [35], Ochiai et al. [36], Anderson [37] with the proposed dual frequency system are summarized in Table 1.

Table 1. Comparisons between the single frequency system with the proposed dual frequency system.

	Tranditional System	**The Proposed System**	**Ratio**	**Remark**
Element spaceing	$d_T \leq \frac{c}{2f}$	$d_P \leq \frac{c}{2(f_2-f_1)}$	$\frac{d_P}{d_T} = \frac{f}{f_2-f_1} \gg 1$	(a)
3 dB Beamwidth	$\theta_T^{3dB} = \frac{0.885c}{Lf}$	$\theta_P^{3dB} = \frac{0.885c}{L(f_2-f_1)}$	$\frac{\theta_P^{3dB}}{\theta_T^{3dB}} = \frac{f}{f_2-f_1} \gg 1$	(b)
FOV	$FOV_T = \frac{c}{df}$	$FOV_P = \frac{c}{d(f_2-f_1)}$	$\frac{FOV_P}{FOV_T} = \frac{f}{f_2-f_1} \gg 1$	(c)
Combining efficiency	$\bar{A}_{\varepsilon_{xT}} = e^{-\left(\frac{\pi f}{c}\right)^2\sigma_x^2}$	$\bar{A}_{\varepsilon_{xP}} = e^{-\left(\frac{\pi(f_2-f_1))}{c}\right)^2\sigma_x^2}$	$\frac{\bar{A}_{\varepsilon_{xP}}}{\bar{A}_{\varepsilon_{xT}}} = e^{\left(\frac{\pi\sigma_x}{c}\right)^2\left(f^2-(f_2-f_1)^2\right)} \gg 1$	(d)
Combining efficiency	$\bar{A}_{\varepsilon_{fT}} = e^{-\left(\frac{1}{12}\left(\frac{L\pi f\sigma_f}{cf_0}\right)^2\right)}$	$\bar{A}_{\varepsilon_{fP}} = e^{-\left(\frac{1}{12}\left(\frac{L\pi(f_2-f_1)\sigma_f}{cf_0}\right)^2\right)}$	$\frac{\bar{A}_{\varepsilon_{fP}}}{\bar{A}_{\varepsilon_{fT}}} = e^{\left(\frac{1}{12}\left(\frac{L\pi\sigma_f}{cf_0}\right)^2\right)\left(f^2-(f_2-f_1)^2\right)} \gg 1$	(e)

Remarks for Table 1:

(a) For a grating-free system, the proposed method provides a larger element spacing than single frequency method which is more suitable for distributed sensor system with large distributed area.

(b) With the same array aperture, the proposed method provides a larger main lobe which can reduce the scanning time.

(c) With the same array aperture, the proposed method provides a larger FOV. Narrow FOV of single frequency system makes it may not work in a practical system with large distributed area.

(d) With the same positioning error, the proposed method provides a higher combining efficiency than single frequency method.

(e) With the same frequency shift, the proposed method provides a higher combining efficiency than single frequency method.

6. Conclusions

Using the phase difference obtained from dual carrier frequency measurements, this paper designs a novel grating lobes-free architecture for distributed sensor system with arbitrary element spacing. Compared with single carrier frequency, the choice of frequency separation in the proposed method is much more flexible. Proper selection of frequency separation can provide the unambiguous DOA estimate in the whole FOV for arbitrary element spacing. The average properties including 3 dB beamwidth, peak and zero points of the sidelobe, 3 dB sidelobe region, and average directivity are derived to evaluate the performance of the proposed architecture in the case of perfect system synchronization. Moreover, beampattern comparisons between the single carrier frequency architecture and the proposed design are also presented in the paper. The effects of the phase ambiguities caused by the imperfect system synchronization is evaluated in terms of the average combining efficiency. Both the average combining efficiencies of the traditional array radar based on single carrier frequency and the proposed architecture are derived for the case with imperfect phase. Theoretical analysis shows the proposed architecture provide a more loose requirements on the precision of system synchronization than the traditional method based on single carrier frequency. An analysis that incorporates the proposed architecture and sensor position diversity technique will be left for a future study.

Author Contributions: Conceptualization, J.H.; methodology, J.H.; software, C.L.; validation, W.H.; formal analysis, J.H. and C.L.; investigation, W.H.; resources, C.L.; data curation, K.L.; writing—original draft preparation, J.H.; writing—review and editing, K.L.; visualization, C.L.; supervision, C.L.; project administration, J.H.; funding acquisition, J.H. All authors have read and agreed to the published version of the manuscript.

Funding: This research was funded by the Fundamental Research Funds for the Central Universities under Grant ZYGX2020ZB030.

Data Availability Statement: Not applicable.

Acknowledgments: The authors would like to thank the anonymous referees for their suggestions and comments.

Conflicts of Interest: The authors declare no conflict of interest.

Abbreviations

The following abbreviations are used in this manuscript:

DOA	Direction of arrival
LO	Local oscillator
SNR	Signal-to-noise ratio
WSN	Wireless sensor networks
MIMO	Multiple-input multiple-output
ULA	Uniform linear array
UCA	Uniform circular array
FOV	Field of view
stds	standard variances
ADC	Analog to digital converter

References

1. Zaidi, S.; Smida, O.B.; Affes, S.; Valaee, S. Distributed Zero-Forcing Amplify-and-Forward Beamforming for WSN Operation in Interfered and Highly Scattered Environments. *IEEE Trans. Commun.* **2020**, *68*, 1187–1199. [CrossRef]
2. Jayaprakasam, S.; Rahim, S.K.A.; Leow, C.Y. Distributed and Collaborative Beamforming in Wireless Sensor Networks: Classifications, Trends, and Research Directions. *IEEE Commun. Surv. Tutor.* **2017**, *19*, 2092–2116. [CrossRef]
3. Diaz, J.D.; Salazar-Cerreno, J.L.; Ortiz, J.A.; Aboserwal, N.A.; Lebron, R.M.; Fulton, C.; Palmer, R.D. A Cross-Stacked Radiating Antenna With Enhanced Scanning Performance for Digital Beamforming Multifunction Phased-Array Radars. *IEEE Trans. Antennas Propag.* **2018**, *66*, 5258–5267. [CrossRef]

4. Mudumbai, R.; Brown Iii, D.R.; Madhow, U.; Poor, H.V. Distributed transmit beamforming: Challenges and recent progress. *IEEE Commun. Mag.* **2009**, *47*, 102–110. [CrossRef]
5. Huang, J.; Wang, P.; Wan, Q. Sidelobe Suppression for Blind Adaptive Beamforming with Sparse Constraint. *IEEE Commun. Lett.* **2011**, *15*, 343–345. [CrossRef]
6. Nerea, D.; David, M.M.; Maria-Pilar, J.A.; Pedro-Jose, G.; Jose-Luis, B.H.; Javier, R.S. Passive Radar Array Processing with Non-Uniform Linear Arrays for Ground Target's Detection and Localization. *Remote Sens.* **2017**, *9*, 756.
7. Lai, Y.P.; Zhou, H.; Zeng, Y.M.; Wen, B. Quantifying and Reducing the DOA Estimation Error Resulting from Antenna Pattern Deviation for Direction-Finding HF Radar. *Remote Sens.* **2017**, *9*, 1285. [CrossRef]
8. Droszcz, A.; Jdrzejewski, K.; Kos, J.; Kulpa, K.; Pooga, M. Beamforming of LOFAR Radio-Telescope for Passive Radiolocation Purposes. *Remote Sens.* **2021**, *13*, 810. [CrossRef]
9. Bollian, T.; Osmanoglu, B.; Rincon, R.; Lee, S.K.; Fatoyinbo, T. Adaptive Antenna Pattern Notching of Interference in Synthetic Aperture Radar Data Using Digital Beamforming. *Remote Sens.* **2019**, *11*, 1346. [CrossRef]
10. Huang, J.; Wan, Q. CRLB for DOA Estimation in Gaussian and Non-Gaussian Mixed Environments. *Wirel. Pers. Commun.* **2013**, *68*, 1673–1688. [CrossRef]
11. Huang, H.; Peng, Y.; Yang, J.; Xia, W.; Gui, G. Fast Beamforming Design via Deep Learning. *IEEE Trans. Veh. Technol.* **2020**, *69*, 1065–1069. [CrossRef]
12. Manteghi, M.; Blanco, R. A Novel Technique for a Low-Cost Digital Phased Array Design. *IEEE Trans. Antennas Propag.* **2013**, *61*, 3495–3501. [CrossRef]
13. Scholnik, D.P. A Parameterized Pattern-Error Objective for Large-Scale Phase-Only Array Pattern Design. *IEEE Trans. Antennas Propag.* **2016**, *64*, 89–98. [CrossRef]
14. Alibakhshikenari, M.; Virdee, B.S.; See, C.H.; Abd-Alhameed, R.A.; Limiti, E. Super-Wide Impedance Bandwidth Planar Antenna for Microwave and Millimeter-Wave Applications. *Sensors* **2019**, *19*, 2306. [CrossRef]
15. Limiti, E. Compact and Low-Profile On-Chip Antenna Using Underside Electromagnetic Coupling Mechanism for Terahertz Front-End Transceivers. *Electronics* **2021**, *10*, 1264.
16. Althuwayb, A.A. Low-Interacted Multiple Antenna Systems Based on Metasurface-Inspired Isolation Approach for MIMO Applications. *Arab. J. Sci. Eng.* **2021**, 1–10. [CrossRef]
17. Althuwayb, A.A. MTM- and SIW-Inspired Bowtie Antenna Loaded with AMC for 5G mm-Wave Applications. *Int. J. Antennas Propag.* **2021**, *2021*, 6658819. [CrossRef]
18. Andreasen, M. Linear arrays with variable interelement spacings. *IRE Trans. Antennas Propag.* **1962**, *10*, 137–143. [CrossRef]
19. Viberg, M.; Engdahl, C. Element position considerations for robust direction finding using sparse arrays. In Proceedings of the Conference Record of the Thirty-Third Asilomar Conference on Signals, Systems, and Computers (Cat. No.CH37020), Pacific Grove, CA, USA, 24–27 October 1999; Volume 2, pp. 835–839.
20. Unz, H. Linear Arrays with arbitrarily distributed elements. *IRE Trans. Antennas Propag.* **1960**, *8*, 222–223. [CrossRef]
21. Ishimaru, A. Theory of unequally-spaced arrays. *IRE Trans. Antennas Propag.* **1962**, *10*, 691–702. [CrossRef]
22. Leahy, R.M.; Jeffs, B.D. On the design of maximally sparse beamforming arrays. *IEEE Trans. Antennas Propag.* **1991**, *39*, 1178–1187. [CrossRef]
23. Holm, S.; Elgetun, B.; Dahl, G. Properties of the beampattern of weight- and layout-optimized sparse arrays. *IEEE Trans. Ultrason. Ferroelectr. Freq. Control* **1997**, *44*, 983–991. [CrossRef]
24. Haupt, R.L. Thinned arrays using genetic algorithms. *IEEE Trans. Antennas Propag.* **1994**, *42*, 993–999. [CrossRef]
25. Murino, V.; Trucco, A.; Regazzoni, C.S. Synthesis of unequally spaced arrays by simulated annealing. *IEEE Trans. Signal Process.* **1996**, *44*, 119–122. [CrossRef]
26. Redlich, R. Iterative least-squares synthesis of nonuniformly spaced linear arrays. *IEEE Trans. Antennas Propag.* **1973**, *21*, 106–108. [CrossRef]
27. Mitrou, N. Results on nonrecursive digital filters with nonequidistant taps. *IEEE Trans. Acoust. Speech Signal Process.* **1985**, *33*, 1621–1624. [CrossRef]
28. Chen, G.H.; Chen, B.X. Eigenstructure-based ambiguity resolution algorithm for distributed subarray antennas VHF radar. *Electron. Lett.* **2012**, *48*, 788–789. [CrossRef]
29. Chen, T.; Wu, Y.; Zhang, W.; Chen, W.; Wang, J.; Hu, Z. Insight Into Split Beam Cross-Correlator Detector With the Prewhitening Technique. *IEEE Access* **2019**, *7*, 160819–160828. [CrossRef]
30. Zoltowski, M.D.; Wong, K.T. Closed-form eigenstructure-based direction finding using arbitrary but identical subarrays on a sparse uniform Cartesian array grid. *IEEE Trans. Signal Process.* **2000**, *48*, 2205–2210. [CrossRef]
31. Li, T.; Nehorai, A. Maximum Likelihood Direction Finding in Spatially Colored Noise Fields Using Sparse Sensor Arrays. *IEEE Trans. Signal Process.* **2011**, *59*, 1048–1062. [CrossRef]
32. Tu, X.; Zhu, G.; Hu, X.; Huang, X. Sparse Sequential Single-Input-Multiple-Output Array Design for Ultra-Wideband Radar. *IEEE Antennas Wirel. Propag. Lett.* **2015**, *14*, 1646–1649. [CrossRef]
33. Roberts, W.; Xu, L.; Li, J.; Stoica, P. Sparse Antenna Array Design for MIMO Active Sensing Applications. *IEEE Trans. Antennas Propag.* **2011**, *59*, 846–858. [CrossRef]
34. Huang, J.; Wang, P.; Wan, Q. Collaborative Beamforming for Wireless Sensor Networks with Arbitrary Distributed Sensors. *IEEE Commun. Lett.* **2012**, *16*, 1118–1120. [CrossRef]

35. Ahmed, M.F.A.; Vorobyov, S.A. Collaborative beamforming for wireless sensor networks with Gaussian distributed sensor nodes. *IEEE Trans. Wirel. Commun.* **2009**, *8*, 638–643. [CrossRef]
36. Ochiai, H.; Mitran, P.; Poor, H.V.; Tarokh, V. Collaborative beamforming for distributed wireless ad hoc sensor networks. *IEEE Trans. Signal Process.* **2005**, *53*, 4110–4124. [CrossRef]
37. Anderson, A.P. Microwave Imaging with Large Antenna Arrays. *Electron. Power* **1984**, *30*, 557. [CrossRef]